Supported Rb-or Cs-containing HPA catalysts for the selective oxidation of isobutane

Li Zhang, Franck Dumeignil, Sébastien Paul, Benjamin Katryniok

▶ **To cite this version:**

Li Zhang, Franck Dumeignil, Sébastien Paul, Benjamin Katryniok. Supported Rb-or Cs-containing HPA catalysts for the selective oxidation of isobutane. Applied Catalysis A : General, 2021, Applied Catalysis A : General, 628, pp.118400. 10.1016/j.apcata.2021.118400 . hal-04094026

HAL Id: hal-04094026
https://hal.univ-lille.fr/hal-04094026v1

Submitted on 23 Oct 2023

HAL is a multi-disciplinary open access archive for the deposit and dissemination of scientific research documents, whether they are published or not. The documents may come from teaching and research institutions in France or abroad, or from public or private research centers.

L'archive ouverte pluridisciplinaire **HAL**, est destinée au dépôt et à la diffusion de documents scientifiques de niveau recherche, publiés ou non, émanant des établissements d'enseignement et de recherche français ou étrangers, des laboratoires publics ou privés.

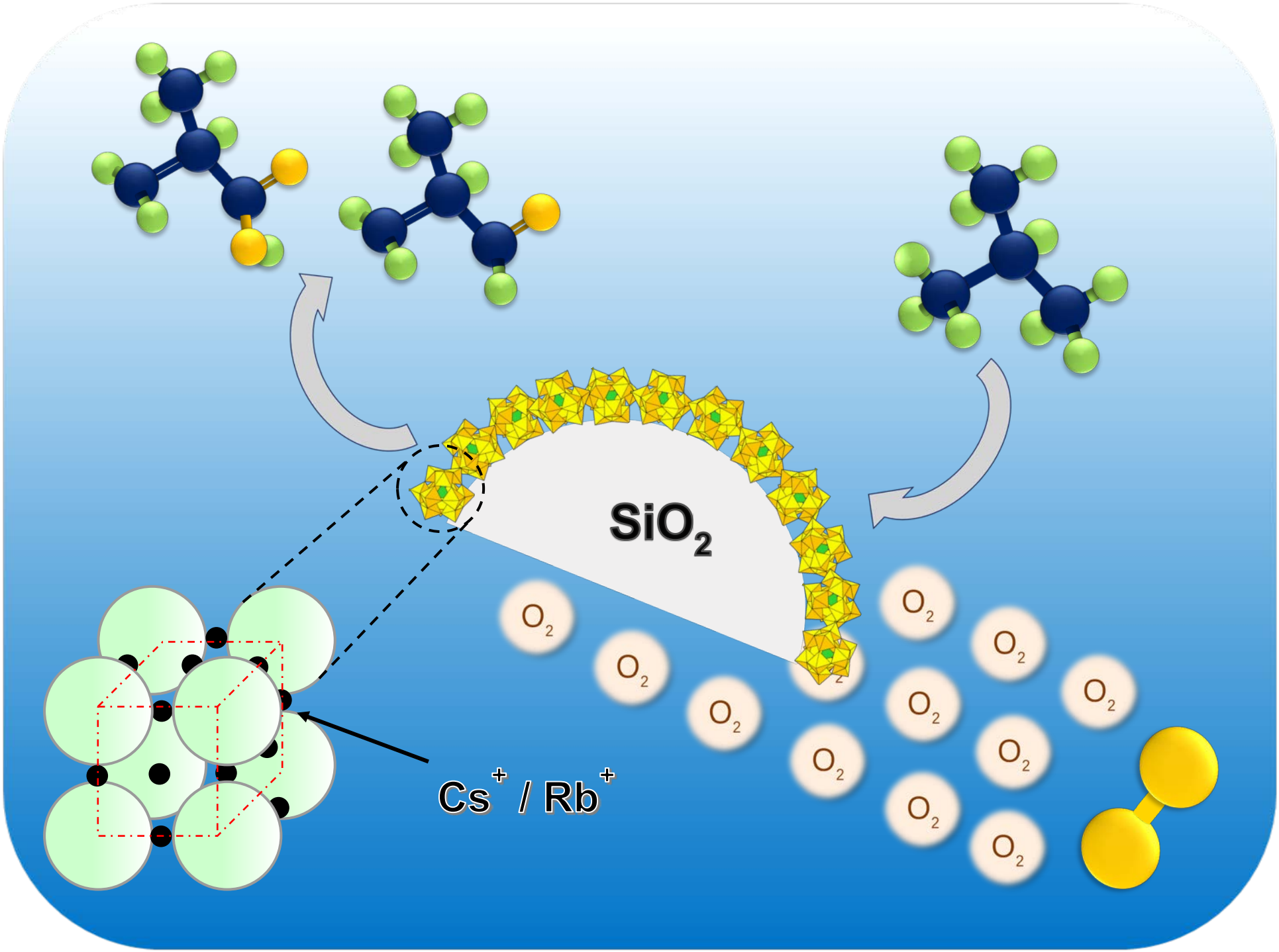
SiO2
O2
O2
O2
O2
O2
O2
O2
O2
O2
O2
O2
Cs+ / Rb+

Supported Rb- or Cs-containing HPA catalysts for the selective oxidation of *iso*butane

Li Zhang, Franck Dumeignil, Sébastien Paul, Benjamin Katryniok*

[a] *Univ. Lille, CNRS, Centrale Lille, Univ. Artois, UMR 8181 – UCCS – Unité de Catalyse et Chimie du Solide, F-59000 Lille, France*

***** Corresponding author: Benjamin Katryniok, benjamin.katryniok@centralelille.fr

Abstract

Silica-supported catalysts based on Keggin-type heteropolyacids (HPAs) containing rubidium or cesium as counter cations have been prepared by the impregnation method and evaluated in the selective oxidation of *iso*butane to methacrolein and methacrylic acid. The catalysts were characterized by various techniques such as XRD, N_2 physisorption, TGA, Raman spectroscopy, H_2-TPR, and NH_3-TPD in order to study their thermal stability, structural, and textural properties, acidity and reducibility. It was evidenced that the reducibility of the Keggin type HPAs was improved by supporting the active phase on SiO_2. A loading of 40 wt.% was the optimum for the selective oxidation of *iso*butane (IBAN) to methacrylic acid (MAA). The selectivities to MAA and methacrolein (MAC) at given conversion were increased when Cs^+ was used as counter cation compared to Rb^+. The same trend was observed for mono- and di-vanado-substituted phosphomolybdic acid, whereby the performance followed the order: CsV_1/SiO_2 > RbV_1/SiO_2 > CsV_2/SiO_2 > RbV_2/SiO_2. The density of acid sites was correlated to the catalytic activity, which underlines the importance of the acid sites for alkane activation.

Keywords: Keggin-type HPA, selective oxidation, *iso*butane, heterogeneous catalysis

1 Introduction

Selective oxidation of light alkanes gives access to valuable oxygenated products such as acrylic acid [1,2], methacrylic acid [3], acetic acid, acrolein, etc. [3–5], which are widely used as monomers in the petrochemical industry [6]. Today, the activation and selective conversion of light alkanes (C_1-C_4) is not only an important research topic for the utilization of natural gas components, but also of practical significance to produce high value-added products. Therefore, the development of new efficient catalysts for the selective oxidation of light alkanes is still of scientific and industrial interest [7,8], notably due to the large availability and cheap costs of the raw materials.

Methacrylic acid (MAA) is an important chemical intermediate, which has two functional groups: a carbon-carbon double bond and a carboxylic acid group. It is used to prepare methyl methacrylate (MMA) for coating, rubber, adhesive, resin, polymer material additives and functional polymer materials. MMA, as a specialty monomer for poly-methyl-methacrylate (PMMA), has been widely used in the fields of architecture, medicine and fine chemicals [9–12]. According to the source of raw materials, the main production for MMA includes the acetone-cyanohydrin (ACH) route and the light hydrocarbons route, from ethylene, propane, propylene, propyne, isobutene, and *iso*butane. Reacting acetone and hydrogen cyanide (HCN) yields MMA (ACH route), which is the most widely used route in Europe and North America, where it is still the dominant commercial process. However, the intermediates (hydrogen cyanide, and acetone cyanohydrin) produced by the ACH process are toxic and source of environmental hazard [13]. Synthesis of MMA through esterification of MAA is an alternative route. Light hydrocarbons, such as C_2, C_3 and C_4 hydrocarbons, were widely developed as feedstocks for MAA. Nevertheless, industrial application was restricted by the harsh reaction conditions, the expensive reactants, the low yields and the relatively high number of reaction steps [14]. Due to the increasing demand for PMMA, the price of MMA monomer increased by 10% annually [12], therefore, to overcome the environmental and production issues linked to the acetone cyanohydrin process, the *iso*butane oxidation method, which would provide a one-step route to form methacrylic acid, has attracted extensive attention because of the easiness of the process and decreased by-product generation [14,15]. Moreover, it is inexpensive and has a lower environmental impact than other fossil feedstocks-based routes and optimally converts *iso*butane to MAA in a single step [16–

19]. With respect to the reaction mechanism, the first step is the catalytic dehydrogenation of *iso*butane to form a C=C double bond. In the following steps, the adjacent methyl group is partially oxidized to a carboxyl group (allylic oxidation). Bifunctional catalysts with acidic and redox properties are necessary to activate the C–H bond [20–23]. Redox properties also have an effect on the oxygen insertion reactions, which generate the oxidized products. Therefore, bifunctional catalysts simultaneously possessing acid and redox properties are necessary.

Heteropolyacids, also known as polyoxometalates (POMs), are nanoscale inorganic metal-oxygen clusters formed by oxygen bonding of pretransition metals (Mo, W, V, Nb, Ta, *etc*.) [24]. Based on the above composition and structural characteristics, Keggin heteropolyacids usually exhibit two properties: Brønsted acidity and oxidative reducibility [25]. The strong Brønsted acidity is related to its highly symmetrical spatial structure. Due to symmetry, cage structure and nanometer size, the negative charge is highly delocalized in the Keggin anion, so that the charge density on the surface is low, the binding ability to proton is weak, and the proton activity is quite high [26–28]. The coordination atoms in Keggin heteropolyacids are generally in their highest oxidation state. Thus, they can be used as multi-electron acceptors with certain oxidation properties. Notably Mo-based heteropolyacids (HPA) accept easily electrons and are reduced to a blue color, named as *"heteropoly blue"*. The initial anion structure is kept after the heteropoly acid is reduced to *"heteropoly blue"*. Heteropolyacid can be reoxidized to recover their initial oxidation state, hence showing a reversible redox property [29].

As aforementioned, selective oxidation of *iso*butane for the production of methyl methacrylate and methacrylic acid has attracted extensive research interest. Selective oxidation of *iso*butane to produce MAC and MAA requires C-H activation, oxidative dehydrogenation, and oxygen insertion. Therefore, the design and development of the catalytic system must focus on the optimization of the parameters influencing the steps of this mechanism. Given that vanadium is known to play a crucial role for both the dehydrogenation and selective oxidation steps of the reaction network, our strategy is focused on the development of a supported Keggin-type HPA catalyst for the selective oxidation of IBAN to MAC and MAA. The heteropoly acid chosen was phosphomolybdic acid $H_3PMo_{12}O_{40}$, which was substituted with V^{5+}. The corresponding vanado-phosphomolybdic acid was furthermore partially

neutralized by Cs^+ counter cations which forms an heteropoly salt presenting a high surface area. Cesium substitution, also increases the hydrophobicity, thus increasing the tendency to expel MAA and MAC, which are polar, resulting thus in increased catalytic performance [30]. Silica was chosen as a support with respect to its larges specific surface area and the fact that it does not have negative impact on the acidity and structure of HPAs [31–33].

To confirm the best loading and optimize the properties of the $Cs_2H_2PMo_{11}VO_{40}/SiO_2$ catalyst, a series of catalysts with 10-50 wt.% loading of $Cs_2H_2PMo_{11}VO_{40}$ (CsV_1) on SiO_2 (CARiACT) was prepared. Similarly, two other series of catalysts $Cs_{2.5}H_{2.5}PMo_{10}V_2O_{40}$ (CsV_2) on SiO_2 and $Rb_{2.5}H_{2.5}PMo_{10}V_2O_{40}$ (RbV_2) on SiO_2 were prepared with the same loadings. Their physicochemical properties and catalytic performances in *iso*butane oxidation were studied. To the best of our knowledge, substitution of H^+ with rubidium (Rb^+) in heteropolyacid has never been investigated before in the selective oxidation of IBAN to MAC and MAA.

2 Experimental section

2.1 Materials syntheses

The formation of $H_4PMo_{11}VO_{40}$ and $H_5PMo_{10}V_2O_{40}$ starts from stoichiometric mixtures [34]. For example, for $H_4PMo_{11}VO_{40}$, 1.42 g of Na_2HPO_4 (Sigma-Aldrich) were dissolved in a solution of 1.22 g of $NaVO_3$ (Fluka) in 50 mL of boiling water (temperature at 100 °C) under stirring. Then, after cooling to room temperature, 1 mL HCl (34-37%, was added and the color turns reddish brown. Following the addition of an aqueous solution of 26.6 g $Na_2MoO_4•2H_2O$ (Alfa Aesar) in 50 mL of water under stirring, the mixture was acidified with 40 mL HCl (34-37%) and the color changed to orange-red. The acidified mixture was kept at room temperature for 5 h and poured into a dividing funnel and then extracted with 70 mL of diethyl ether. The extraction was accomplished by repeated shaking, after which the layers separated. The HPA etherate in the lowest layer was isolated, 7 mL of water was added and kept for crystallization at room temperature. The yield was 20 g, calculated for $H_4PMo_{11}VO_{40}•30.5H_2O$.

The CARiACT® SiO_2 (Q-10), commercially available from Fuji Silysia Chemical Company, was used as a support. The preparation of 10-50 wt.% $Cs_2H_2PMo_{11}VO_{40}$, $Rb_2H_2PMo_{11}VO_{40}$, $Cs_{2.5}H_{2.5}PMo_{10}V_2O_{40}$ and $Rb_{2.5}H_{2.5}PMo_{10}V_2O_{40}$ supported on SiO_2 was carried out in two steps [35]:

1) SiO_2 was impregnated with Cs_2CO_3 (Fluka) or Rb_2CO_3 (Aldrich). The support and 30 mL of 100% ethanol were stirred at 60 °C. Then, the desired amount of Cs_2CO_3 or Rb_2CO_3 was added. After 30 min, the solvent was evaporated under vacuum at 60 °C for 1.5 h. *2)* The as-prepared support was then impregnated with HPA: after suspending in 30 mL of 100% ethanol was subsequently added the required amount of HPA ($H_4PMo_{11}VO_{40}$ or $H_{.5}PMo_{10}V_2O_{40}$) dissolved in a minimum quantity of ethanol. After 30 min, the solvent was evaporated under vacuum at 60 °C until the obtained solid was dry.

In order to make comparisons easier between the different catalysts, the formulation of the series of catalysts $Cs_2H_2PMo_{11}VO_{40}/SiO_2$, $Cs_{2.5}H_{2.5}PMo_{10}V_2O_{40}/SiO_2$ and $Rb_{2.5}H_{2.5}PMo_{10}V_2O_{40}/SiO_2$ are labelled in the followings as CsV_1/SiO_2, CsV_2/SiO_2 and RbV_2/SiO_2, respectively, where CsV_1 or CsV_2 or RbV_2, is the active phase of the catalyst and SiO_2 is the support of the catalyst. Catalysts with different mass of active phase on SiO_2 support *x* wt.% $Cs_2H_2PMo_{11}VO_{40}/SiO_2$, *x* wt.% $Cs_{2.5}H_{2.5}PMo_{10}V_2O_{40}/SiO_2$ and *x* wt.% $Rb_{2.5}H_{2.5}PMo_{10}V_2O_{40}/SiO_2$ are labelled in the following as $xCsV_1$, $xCsV_2$ and $xRbV_2$, respectively, where *x* ranges from 10 to 50.

2.2 Characterization

Optical microscope images were obtained using a ZEISS Axio Lab. A1 equipped with a 5x objective (ZEISS EC EPIPLAN) and 10x eyepieces, a differential interference contrast (C-DIC) and a professional microscope camera AxioCam ERc 5s equipped with a 5MP CMOS Sensor giving a resolution of 2560 (H) × 1920 (V).

Thermogravimetric analysis (TGA) was performed using a SETARAM instruments to study the thermal decomposition behavior of the catalysts. The catalysts were heated from 20 °C to 700 °C at a rate of 3 °C/min under air flow.

X-ray diffraction patterns (XRD) were recorded in ambient conditions using the CuKα radiation (λ = 1.5418 Å; 40 kV, 30 mA) on a Siemens D5000 diffractometer, with a 0.02° scan step and 1 s time step in the 10-80° range. The interpretation of the diffractograms was performed using the Diffrac Eva software and by comparison by JCPDS reference files.

IR-Raman spectra were collected on a Horiba Xplora using a laser beam of 532 nm wavelength for excitation in confocal mode. A 50x long working distance objective (Olympus) was used for both

focusing the excitation beam on the sample and collecting the scattered light. The latter was dispersed using an 1800 grooves spectrometer grating after having passed through a confocal hole of 300 µm. A Peltier-cooled CCD detector was used for recording the Raman spectra.

The Brunauer-Emmett-Teller (BET) model serves as the basis for the measurement of the specific surface area of materials. N_2 physisorption isotherms at liquid nitrogen temperature were obtained on a TriStar II Plus gas adsorption analyzer (Micromeritics) after outgassing at 130 °C in vacuum overnight. Specific surface areas were evaluated with the BET model over the following range: P/P_0 = 0.05-0.30. The total pore volume was measured from the volume of N_2 adsorbed at P/P_0 = 0.95.

Temperature-programmed reduction (TPR) analyses were conducted with an automated AutoChem II 2920 Chemisorption Analyzer from Micromeritics. 100 mg of catalyst were inserted into a glass reactor. The sample was flushed with a gas mixture comprising 5 Vol.% H_2 in Ar at room temperature with a flow rate of 50 mL/min STP. The temperature of the sample was increased linearly at a ramp rate of 5 °C/min up to 1000 °C. The consumption of hydrogen was monitored *via* a TCD signal converted by use of a calibration factor, to get quantitative information on the species present in the catalyst.

Ammonium temperature-programmed desorption (NH_3-TPD) with mass spectrometry (MS) was performed to quantify the amount and strength of the acidic sites of the catalysts. A typical test was as follows: 50 mg catalyst were pre-treated in a He flow (30 mL/min) at 130 °C for 2 h in order to remove the physisorbed water. Then, NH_3 was absorbed at the surface by pulsed injections at 130 °C until saturation was stated from the MS signal. The TPD profiles were monitored by MS and thermal conductivity detector and recorded from 130 to 650 °C at a heating rate of 10 °C/min.

2.3 Catalytic oxidation of *iso*butane

The catalytic reactions for the selective oxidation of *iso*butane to methacrolein and methacrylic acid were performed in a fixed-bed reactor under atmospheric pressure. The reactor was loaded with 0.8 g of catalyst sandwiched by carborundum (SiC, 0.21 mm diameter) to keep the catalytic bed in the isothermal zone of the reactor. The reactor was heated to reaction temperature at a 5 °C/min heating rate. The reactants mixture was fed at a constant total flow-rate of 10 mL/min STP (molar ratio 28% IBAN; 12% O_2; 10% H_2O; 50% He), corresponding to a WHSV (weight hourly space velocity) of 0.75

$L \cdot g^{-1} \cdot h^{-1}$. Water was introduced via a saturation system keeping 10% partial pressure of water in the gas stream. All products were analyzed on-line by gas chromatography (GC). The reaction data were obtained under stream at steady state conditions.

3 Results and discussion

3.1 Physicochemical properties of the catalysts

3.1.1 Microstructure of the catalysts

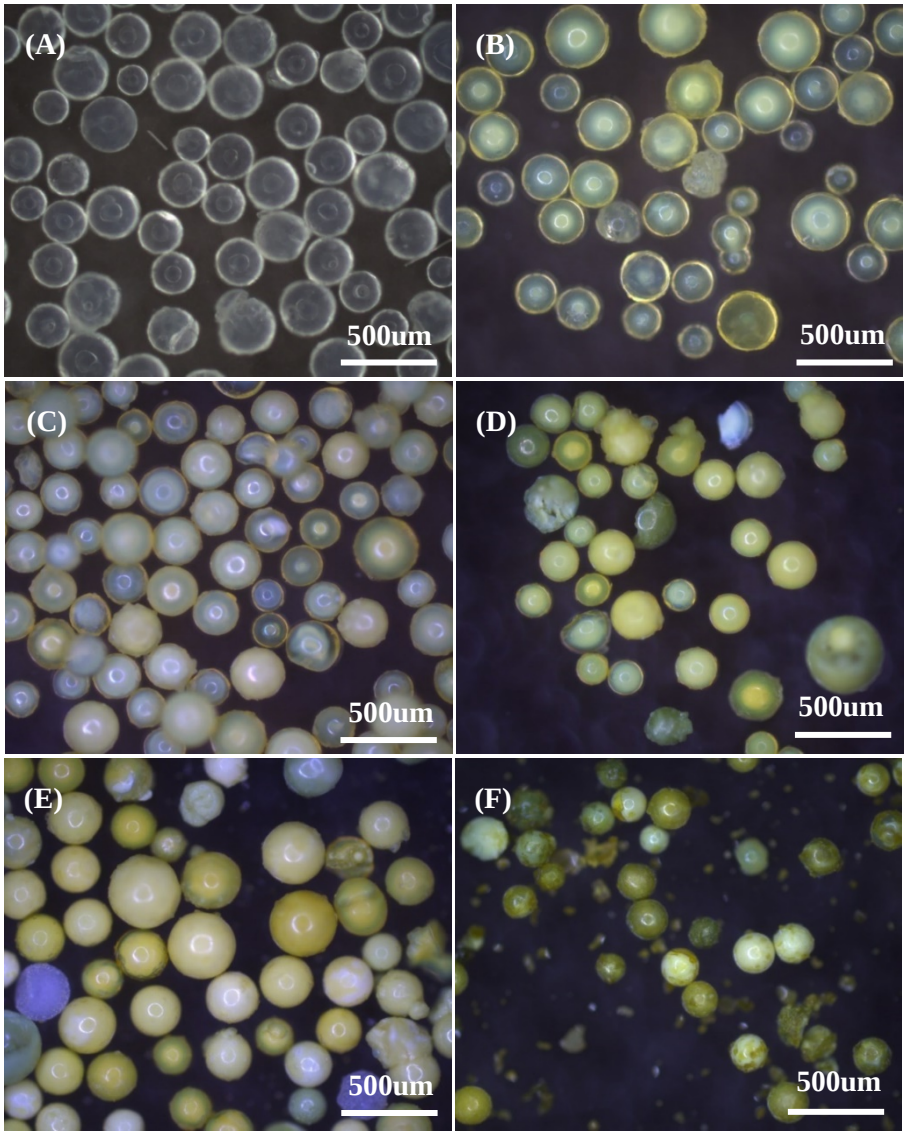

Fig. 1. Typical optical microscope images of SiO_2 and $x CsV_1$ spheres with x = 10 to 50. (A) SiO_2, (B) $10CsV_1$, (C) $20CsV_1$, (D) $30CsV_1$, (E) $40CsV_1$, (F) $50CsV_1$.

Fig. 1 shows the typical optical microscope images of SiO_2 and $x CsV_1/SiO_2$ spheres with x = 10 to 50. It indicates that the CARIACT SiO_2 spheres possess good uniformity with an average size of ~200 μm as expected (**Fig. 1A**). After coating of CsV_1 active phase, core–shell CsV_1/SiO_2 spheres

were formed, which maintain similar uniformity. Upon increasing the amount of active phase, the colors of the surfaces of the CsV_1/SiO_2 spheres change progressively from white to yellow. For the 10 wt.%-20 wt.% loadings (**Fig. 1B and C**), a bright yellow shell is observed, while for the 30 wt.% - 40 wt.% loadings (**Fig. 1D and E**) the yellow color is more homogeneous. For the 50 wt.% loading (**Fig. 1F**), the shell became too thick and detaches from the silica surface, whereby small pieces of debris (CsV_1) were clearly visible on the micrograph. Similar results, were obtained for CsV_2/SiO_2 and RbV_2/SiO_2 catalysts (not shown).

3.1.2 Thermal decomposition of the fresh catalysts TGA

According to the thermogravimetric curve in **Fig. 2**, the weight loss of the catalysts can be divided into two stages. The first stage is at temperatures below 100 °C. Here, the weight loss is caused by the evacuation of physisorbed water. The second weight loss - observed in the 150 °C to 340 °C range - is caused by the loss of crystal water which is in agreement with literature [36], reporting that phosphomolybdic acid loses its constitution water at 375 °C. Furthermore, these results evidence that below 400 °C, the catalyst only loses crystal water, but no constitution water, whereby the acidic protons are retained, which is important with respect to the chosen reaction temperature (< 400 °C).

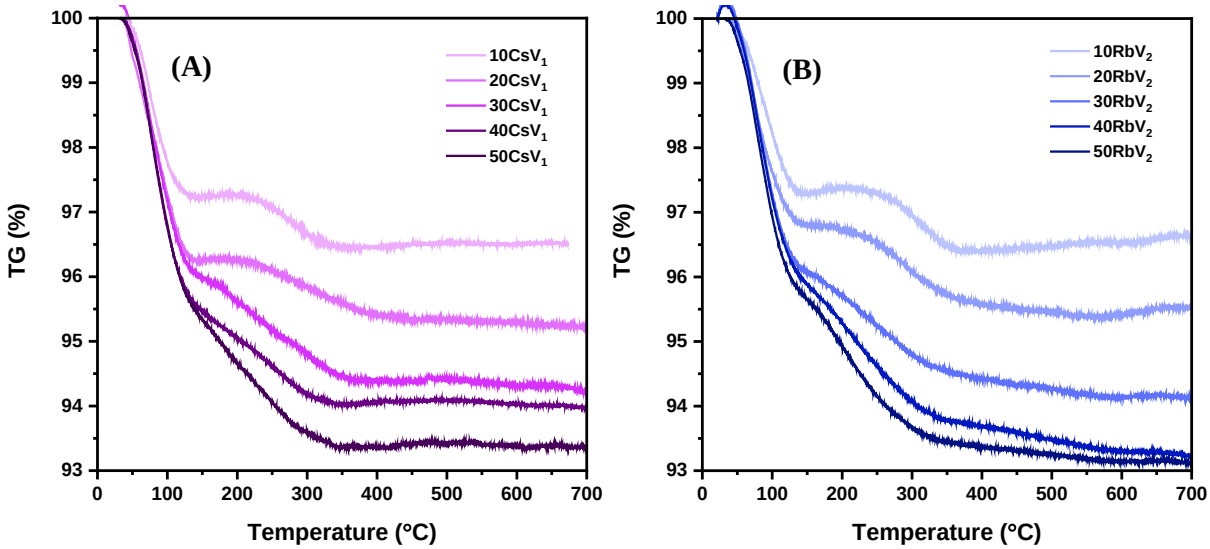

Fig. 2. TGA curves of the series of catalysts (A) CsV_1/SiO_2 catalysts, (B) RbV_2/SiO_2 catalysts.

3.1.3 Crystal phases analysis of the samples XRD

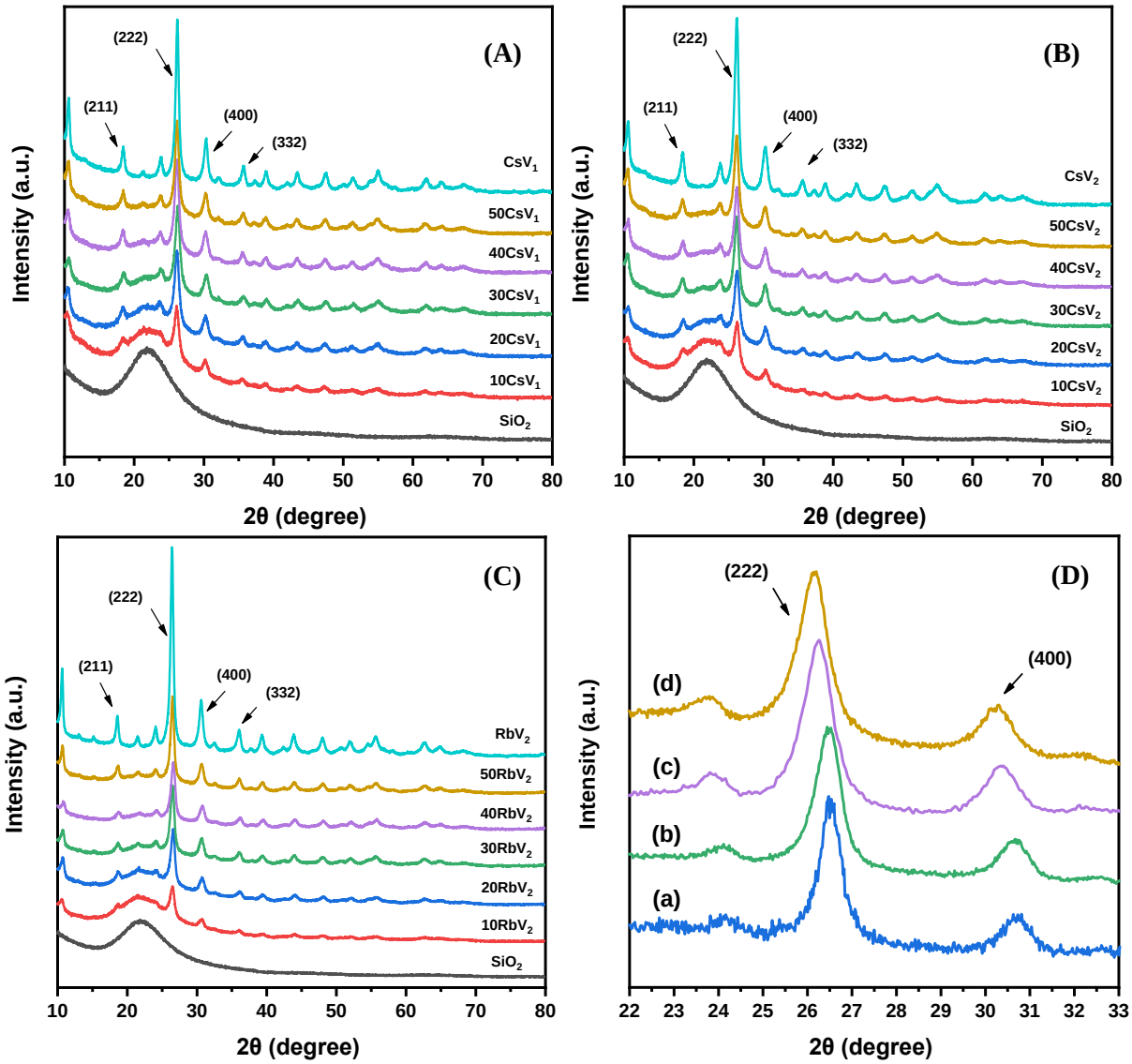

Fig. 3. XRD patterns of (A)SiO_2 and CsV_1/SiO_2 catalysts, (B)SiO_2 and CsV_2/SiO_2 catalysts, (C)SiO_2 and RbV_2/SiO_2 catalysts with various loadings: 10-50 wt.%, (D) Catalysts with loading 30 wt.%: (a) $30RbV_1$, (b) $30RbV_2$, (c) $30CsV_1$, (d) $30CsV_2$.

Fig. 3 shows the typical XRD patterns of SiO_2, CsV_1/SiO_2 catalysts (**Fig. 3A**), CsV_2/SiO_2 catalysts (**Fig. 3B**) and RbV_2/SiO_2 catalysts (**Fig. 3C**). The patterns exhibit diffraction peaks at 2θ = 18.5°, 23.9°, 26.2°, 30.4° and 35.8° assigned to the lattice planes of (211), (310), (222), (400), and (332) of both cubic CsV_1/SiO_2 and CsV_2/SiO_2 catalysts, respectively, which are characteristic for Keggin-type compounds. For RbV_2/SiO_2 catalysts, the observed diffraction peaks at 2θ = 18.6°, 24.1°, 26.5°, 30.7° and 36.2° can be assigned to the lattice planes of (211), (310), (222), (400), and (332), respectively. With the increase in active phase amounts, the intensities of the diffraction peaks corresponding to the lattice planes of (211), (310), (222), (400), and (332) belonging to Keggin-type

compounds were largely enhanced, suggesting the presence of large amounts of active phase on SiO_2. As a matter of fact, the interplanar spacing was then expanded as Cs^+ has a larger ionic radius than Rb^+, ascribed to *d*-spacing decrease when the protons were substituted by Rb cations in comparison with by Cs cations. The *d*-spacing of the (222) plane increased from 0.3362 nm for $Rb_2H_2PVMo_{11}O_{40}$ to 0.3393 nm for $Cs_2H_2PMo_{11}VO_{40}$. Therefore, the diffraction peaks of Rb-containing catalysts were slightly shifted to the higher angles in comparison with the diffraction peaks of Cs-containing catalysts, could be clearly observed in **Fig. 3D**.

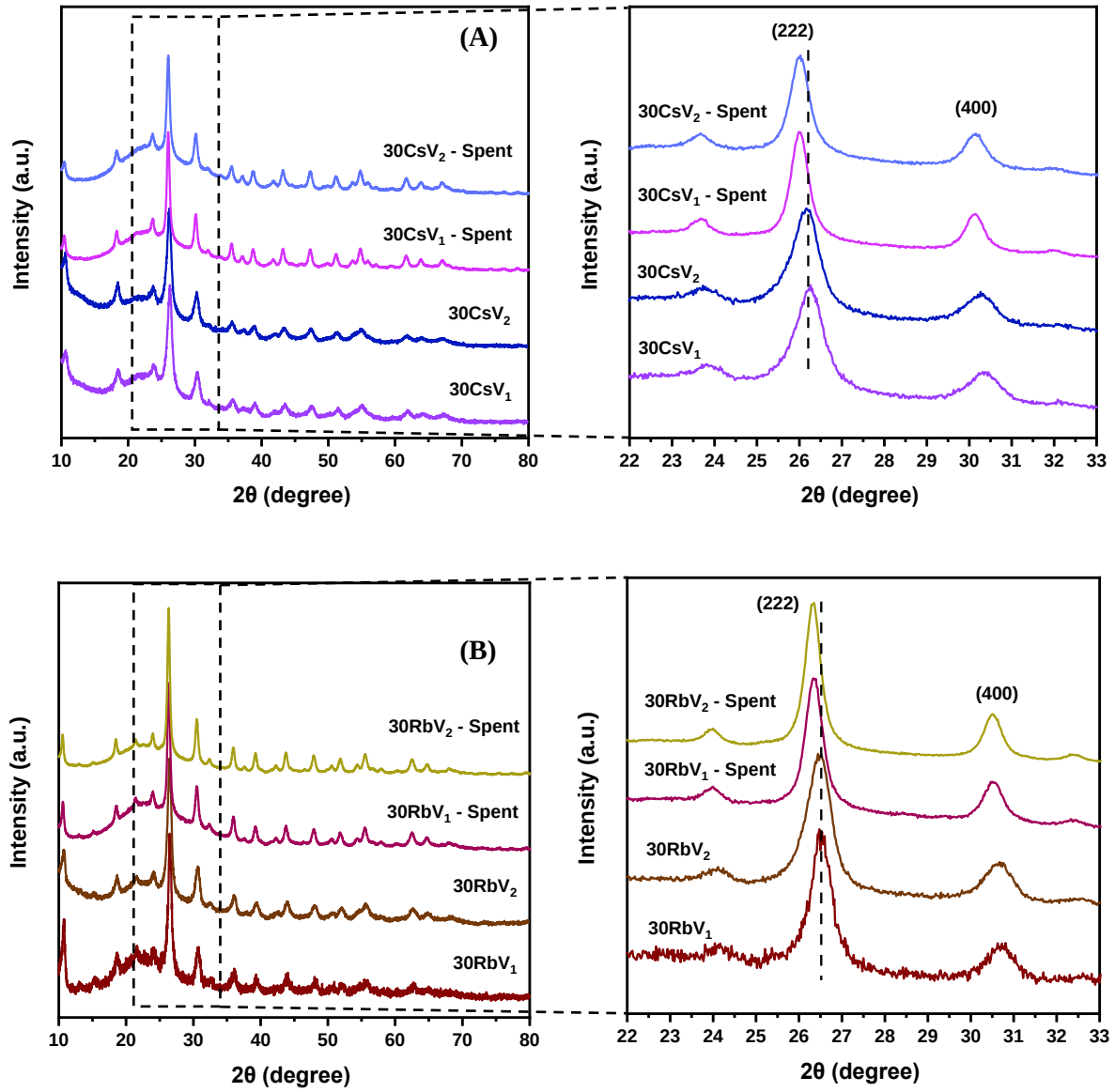

Fig. 4. XRD patterns of fresh and spent catalysts: (A) $30CsV_1$ and $30CsV_2$ catalysts, (B) $30RbV_1$ and $30RbV_2$ catalysts.

Fig. 4 shows the XRD patterns of the catalysts with 30 wt.% before and after reaction. It is worth mentioning that there was no new diffraction peak in the spent catalysts, which indicated that the catalysts did not decompose into metal oxides during the reaction process, which also indicated that the catalysts were quite stable under the reaction conditions. However, the diffraction peak of the spent catalyst is slightly shifted towards a small angle, by 0.2°. As shown for the lattice plane of (222), the diffraction peak of the Cs-containing catalyst is shifted from 26.2° to 26.0°, same for the Rb-containing catalyst (also from 26.2° to 26.0°). This was accounted for the loss of crystal water which led to a small modification of the lattice parameter, which is also consistent with the results of TG analysis [37]. It should also be noted that the diffraction peaks of the spent catalyst become narrower compared to those of the fresh one, implying an increase in crystallinity of the catalyst after reaction, probably due to sintering. This proposal is consistent with that observed in the BET results, with a slight decrease in the specific surface area of the spent catalysts compared to the fresh ones (**Table S1**).

3.1.4 BET specific surface area and pore volume of the catalysts

The specific surface areas of the SiO_2 (CARIACT) support and of the catalysts are gathered in **Table 1**. The surface area of the catalysts decreased with increasing the amount of active phase, from 264.2 m^2/g (SiO_2 support) to 150.9 m^2/g ($50CsV_1$), 197.8 m^2/g ($50CsV_2$) and 194.2 m^2/g ($50RbV_2$), respectively. Theoretical values obtained from the calculation (assuming that the active phase was well and homogeneously dispersed as referred to [14]) is also given in brackets in **Table 1**. When comparing the experimental and theoretical BET values, it can be seen that all the catalysts display a higher specific surface area than the calculated theoretical one. This indicates that the active phase (CsV_1, CsV_2, RbV_2) partially contributes to the catalysts surface area and that new surface is created due to the porous structure of the active phase.

The mean value of the coverage of active phase on the support for the different loadings was calculated based on a Keggin unit occupancy of 1.44 nm^2 [31,38]. In **Table 1** the average coverage of the support expressed as the number of active phase layers stacked on the surface is reported. Based on the surface area of the CARiACT®-SiO_2 (264.2 m^2/g), a theoretical CsV_1 monolayer coverage (0.8-1.3 layers) was reached for a loading of 30-40 wt.%. This theoretical monolayer indicates a homogenous distribution of the active phase on the support, as evidences by optical microscopy.

Table 1.

Textural properties of the supported catalysts and coverage of active phase.

Catalysts	**SiO_2** (CARIACT)	**$10CsV_1$**	**$20CsV_1$**	**$30CsV_1$**	**$40CsV_1$**	**$50CsV_1$**	**CsV_1**
S_{BET}, m^2/g	264.2	233.0 (237.8)[a]	226.0 (211.4)[a]	219.8 (184.9)[a]	179.4 (158.5)[a]	150.9 (132.1)[a]	70.4
V_{pore}, cm^3/g	1.12	0.94	0.81	0.69	0.49	0.4	0.05
Catalysts		**$10CsV_2$**	**$20CsV_2$**	**$30CsV_2$**	**$40CsV_2$**	**$50CsV_2$**	**CsV_2**
S_{BET}, m^2/g	- -	242.3 (237.8)[a]	234.9 (211.4)[a]	217.5 (184.9)[a]	215.0 (158.5)[a]	197.8 (132.1)[a]	122.3 -
V_{pore}, cm^3/g	-	0.96	0.81	0.66	0.6	0.46	0.09
Catalysts		**$10RbV_2$**	**$20RbV_2$**	**$30RbV_2$**	**$40RbV_2$**	**$50RbV_2$**	**RbV_2**
S_{BET}, m^2/g	- -	236.1 (237.8)[a]	232.3 (211.4)[a]	215.2 (184.9)[a]	206.3 (158.5)[a]	194.2 (132.1)[a]	120.1 -
V_{pore}, cm^3/g	-	0.94	0.82	0.68	0.65	0.48	0.08
Coverage, layer	-	0.2	0.5	0.8	1.3	1.8	

[a] theoretical values were calculated according to the specific surface area of SiO_2 measured in the same conditions: $S_T = S_{BET\text{-}SiO2} \times (100 - x)$ with x in wt.%.

3.1.5 Structural features of the catalysts observed by Raman spectroscopy

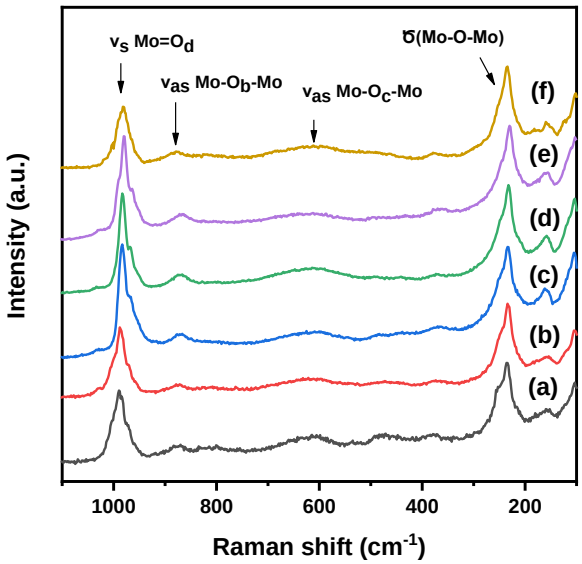

Fig. 5. Raman spectra for the series of $Cs_2H_2PMo_{11}VO_{40}/SiO_2$ catalysts (a) 10 wt.%, (b) 20 wt.%, (c) 30 wt.%, (d) 40 wt.%, (e) 50 wt.%, (f) bulk active phase.

The CsV_1 series of catalysts has been studied using Raman spectroscopy (**Fig. 5** and **Fig. S1**) to further confirm the integrity of the Keggin structure in the salt of the HPA samples. The observed bands corresponded to the characteristic Keggin feature bands at the following vibrations [14,39]: *ν*s Mo=O_d at 983 cm^{-1}, *ν*as Mo-O_b-Mo at 871 cm^{-1}, *ν*as Mo-O_c-Mo at 600 cm^{-1} and *δ*(Mo-O-Mo) 255 and 235 cm^{-1}, respectively. The P-O vibration in Keggin units is Raman-inactive [40]. This also indicates that the Keggin structure of the catalyst has been effectively formed. Nevertheless, the signal of V-O

bonds was not observed, which may be explained by the low amount of vanadium in the catalysts which is in agreement with the literature [14].

3.1.6 Reducibility measurements using TPR

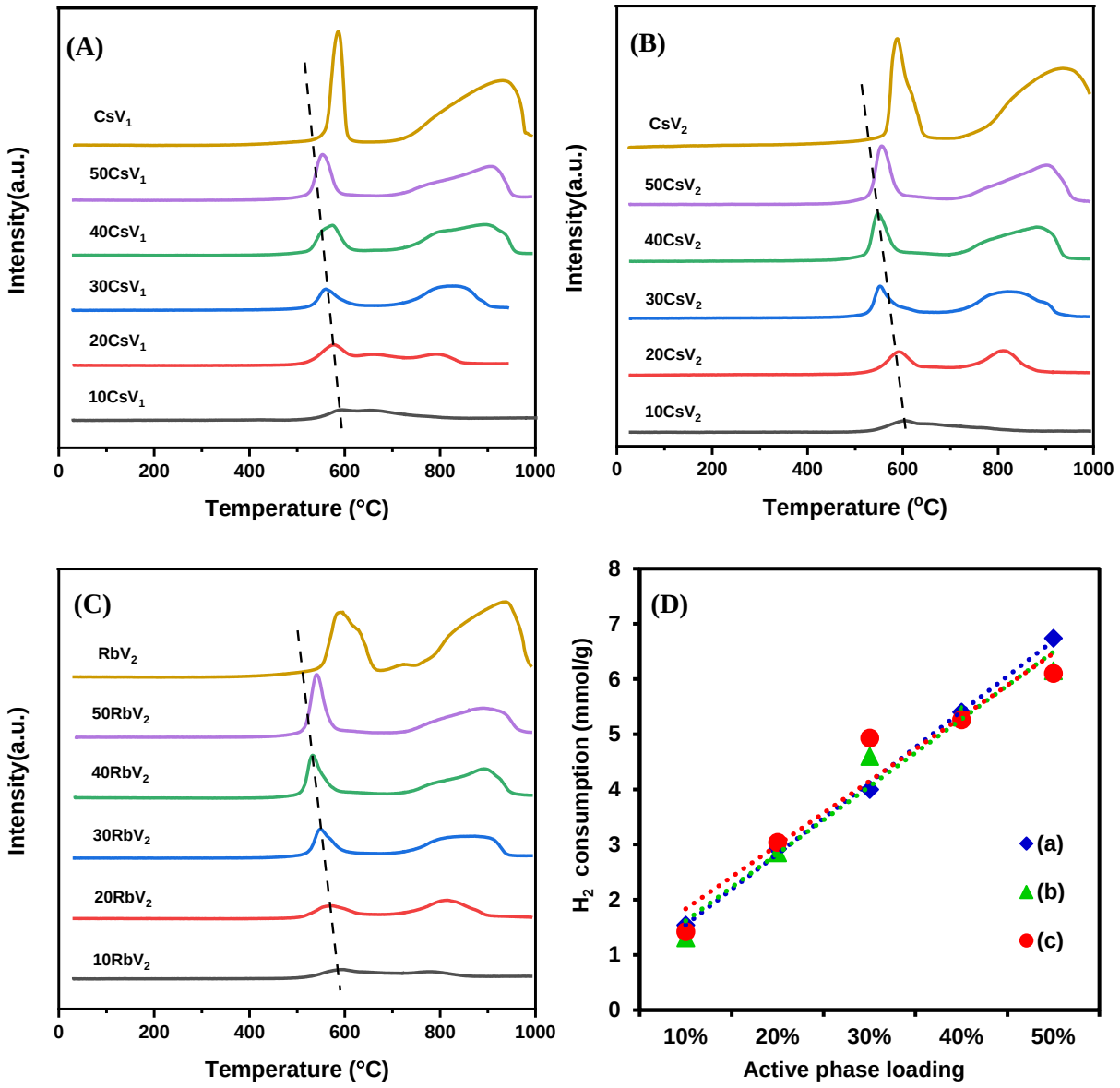

Fig. 6. TPR profiles of the catalysts: (A) CsV_1 and CsV_1/SiO_2 catalysts, (B) CsV_2 and CsV_2/SiO_2 catalysts, (C) RbV_2 and RbV_2/SiO_2 catalysts with various loadings: 10-50 wt.%, (D) H_2 consumption as a function of active phase loading for the three series of catalysts (a) CsV_1/SiO_2 catalysts, (b) CsV_2/SiO_2 catalysts, (c) RbV_2/SiO_2 catalysts.

Fig. 6 shows the reducibility of the three series of catalysts, which were examined by H_2-TPR measurements. The reduction at lower temperatures starting from 550 °C is ascribed to the first step of the reduction of the Mo^{6+} species (from tetrahedral Mo^{6+} to Mo^{4+}). The reduction peak at the higher temperature of approximately from 800 °C was attributed to the reduction of the tetrahedral Mo^{4+} to Mo^0 [41]. The broad peaks observed hereby indicated a rather complex reduction process composed

of one or more transition states [14]. Concerning vanadium, the content was too low to observe its reduction which should occur at a lower temperature. As one can see from **Fig. 6D**, the H_2 consumption increased linearly with the loading, indicating that all Mo was accessible for reduction. It is noteworthy that with the increase in the loading (10-40 wt.%), the reduction peak shifted to lower temperature, before shifting back when the loading reached 50 wt.%, indicating that the catalyst with 40 wt.% exhibited the highest reducibility.

3.1.7 Quantification and strength of the acid sites by NH_3 TPD

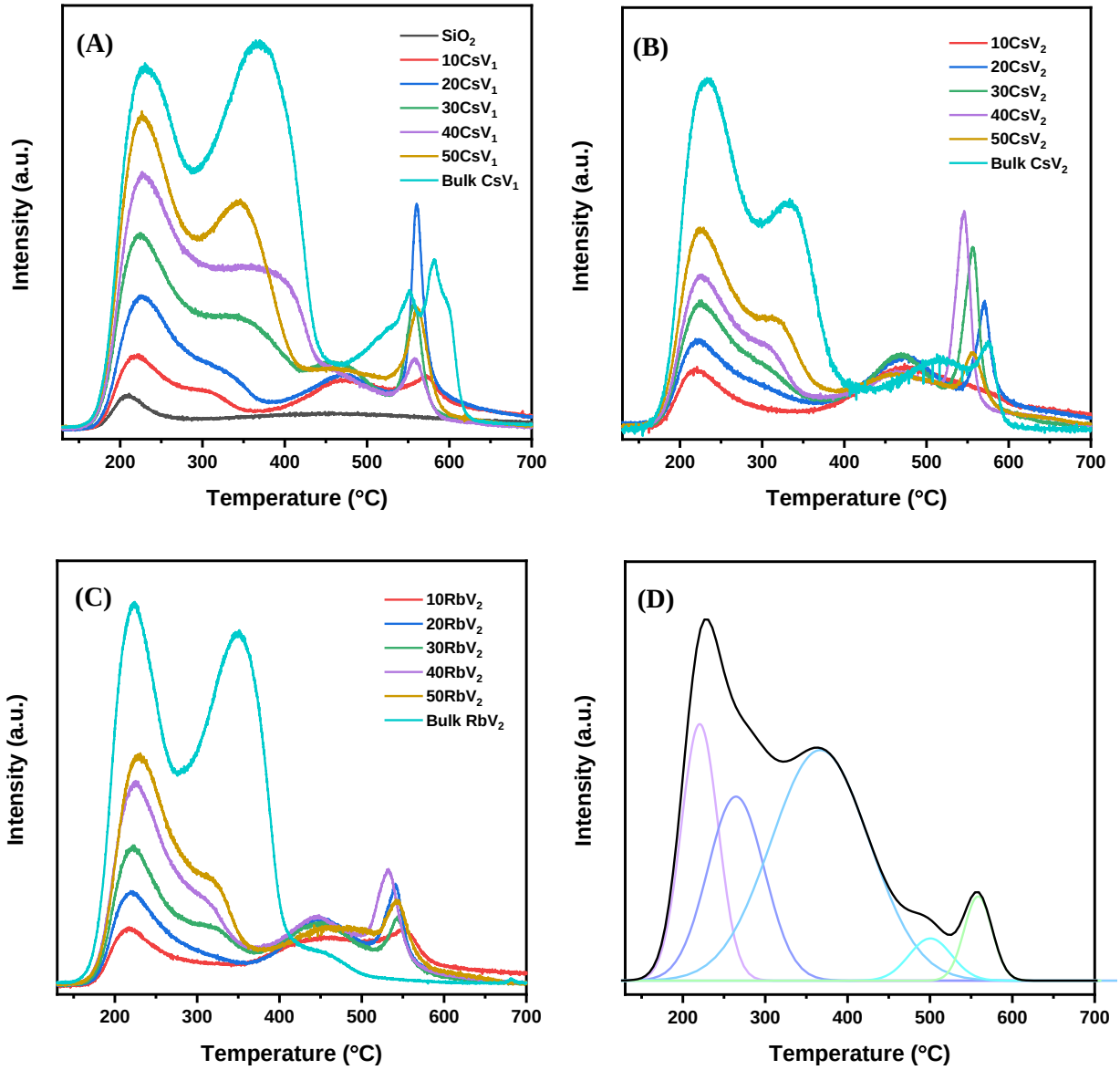

Fig. 7. NH_3-TPD profiles for: (A) CsV_1 and CsV_1/SiO_2 catalysts, (B) CsV_2 and CsV_2/SiO_2 catalysts, (C) RbV_2 and RbV_2/SiO_2 catalysts with various loadings: 10-50 wt.%, (D) NH_3-TPD deconvolution curve of $40CsV_1$ sample taken as an example.

The amount and strength of acid sites of the three series of catalysts (xCsV$_1$/SiO$_2$, xCsV$_2$/SiO$_2$ and xRbV$_2$/SiO$_2$ catalysts) were determined by temperature-programmed desorption of ammonia (NH_3-TPD). The desorption temperature profiles are plotted in **Fig. 7** and the quantitative calculation for the NH_3 uptake are listed in **Table S2**. For silica, a small desorption peak was observed, which indicates that the support has no acidity. For the three series of silica-supported catalysts, four NH_3 desorption peaks could be distinguished: weak acid sites (100-300°C), medium acid sites (300-450°C), strong acid sites (450-560°C) and very strong acid sites (560-700°C) [38]. However, no clear tendency regarding the distribution of acid strength was found in these series. On the other hand, concerning the total amount of acid sites, the latter increased with the amount of active phase. For $Cs_2H_2PMo_{11}VO_{40}/SiO_2$ catalysts, for example, from 10 wt.% to 50 wt.%, the ammonia uptakes were 0.16, 0.28, 0.34, 0.46 and 0.50 mmol/g, respectively. However, for lower loadings, the number of acid sites of the catalysts increased significantly, but only moderately for higher loadings from 40% to 50 wt.% (**Fig. 8**A). This was ascribed to overloading with active phase leading to non-accessible sites and the formation of isolated detached bulk CsV_1, as evidenced in the microscope images. By comparing the three series of catalysts, we found that the CsV_1/SiO_2 series exhibited the higher amount of acid sites, followed by the CsV_2/SiO_2 series catalysts, and the RbV_2/SiO_2 series ((**Fig. 8B**).

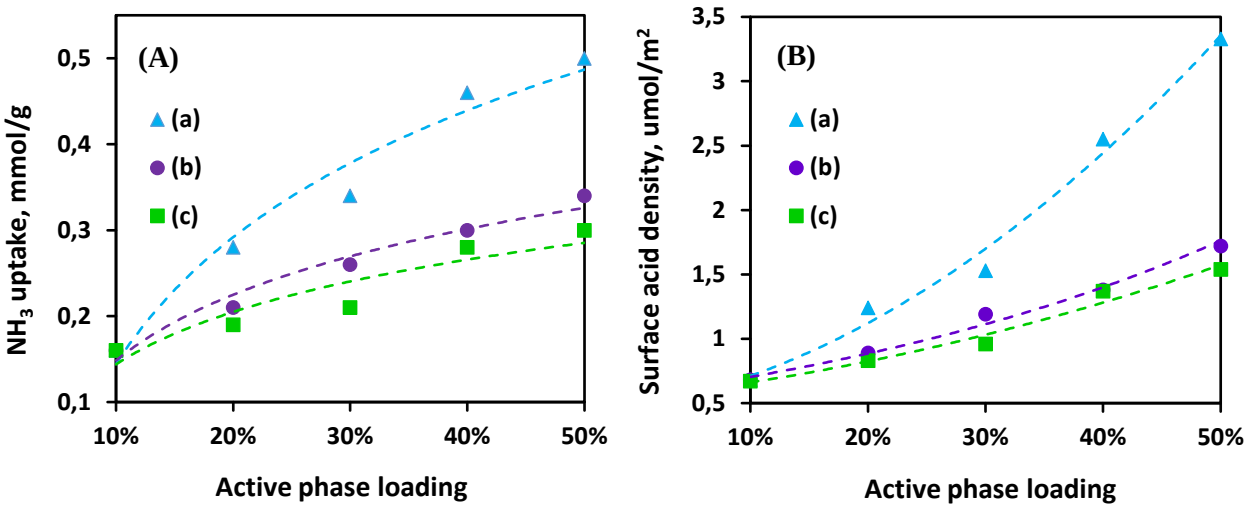

Fig. 8. (A) Amount of acid sites as a function of the active phase loading. (B) Relationship between the active phase loading and the surface acid density: (a) CsV_1/SiO_2 catalysts, (b) CsV_2/SiO_2 catalysts, (c) RbV_2/SiO_2 catalysts.

3.2 Catalytic evaluation in *iso*butane oxidation reaction

3.2.1 Effect of the support

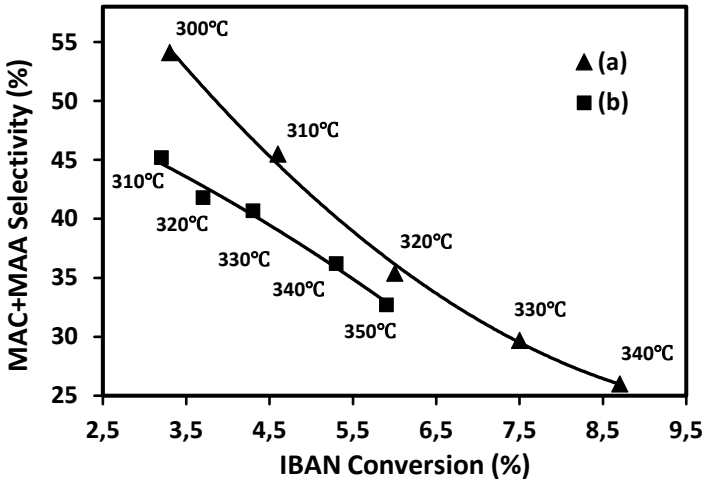

Fig. 9. Relationship between IBAN conversion and selectivity (MAC+MAA) of (a) $30CsV_1$, (b) pure CsV_1 at different temperature.

The catalytic performance of all the series of catalysts was evaluated in the selective oxidation of *iso*butane to MAC and MAA in the same operating conditions (**Fig. 9**). The lowest IBAN conversion (X_{IBAN} = 3.7 %) was found for 0.24 g of bulk CsV_1, this mass corresponding to the amount of active phase in the $30CsV_1$ catalyst (**Table S3**). This low conversion was related to the rather low specific surface area (70.4 m^2/g) of the sample. Furthermore, it was found that the bulk catalyst was unstable, becoming over-reduced under the reaction conditions as evidenced by a color change to green-blue after reaction, whereas the supported catalyst remains yellow-green. After supporting the CsV_1 active phase over CARiACT®-silica, the catalytic activity was increased to X_{IBAN} = 6.0 % for the $30CsV_1$ catalyst.

3.2.2 Effect of the active phase and reaction temperature

The catalytic performances of the catalysts with a constant amount of 30 wt.%. of active phase on SiO_2 support, namely $30CsV_1$, $30CsV_2$, $30RbV_1$ and $30RbV_2$ were studied and reported in **Fig. 10** and **Tables S4 to S7**. In addition, in all cases, the carbon balance was >99.5%, which means that at least 95% of the product was detected even at low *iso*butane conversion. The *iso*butane conversion over the four kinds of catalysts increased with the reaction temperature, as expected. Maximum conversions of 8.7% for the $30CsV_1$ catalyst at 340 °C, 7.7% for the $30CsV_2$ catalyst, 7.3% for the

$30RbV_1$ catalyst and 5.5% for the $30RbV_2$ catalyst at 350 °C were observed. As one can see, the reaction temperature is a key factor that affects the catalytic activity. At higher temperature, the IBAN conversion increased, but this increase was accompanied by the over-oxidation of the products. In fact, large selectivity to CO_2 was found whereas the selectivity to the main products of interest, namely MAC and MAA, decreased. For the by-products acetic acid and acetone, the selectivity has an opposite trend with respect to temperature according to **Tables S4 to S7**. Acetone also decomposes further with increasing temperature to form C2 and C1. This result, is in agreement with Busca *et al.*,[42,43] postulating a reaction network for the formation the by-products, where the oxidative degradation of MAA and MAC to AA and CO_2 is responsible for the decrease in desired products. The reaction network was also proposed by Paul *et al.* [44,45], who claimed that MAC, MAA and degradation products were formed through parallel reactions from *iso*butane directly. At a high reaction temperature, more over-oxidation products are produced, resulting in the formation of less desired products since the degradation of MAC was around 50 times faster than *iso*butane activation. Therefore, maintaining the high selectivity of the desired product requires that the temperature of the oxidation operation should be appropriately lowered.

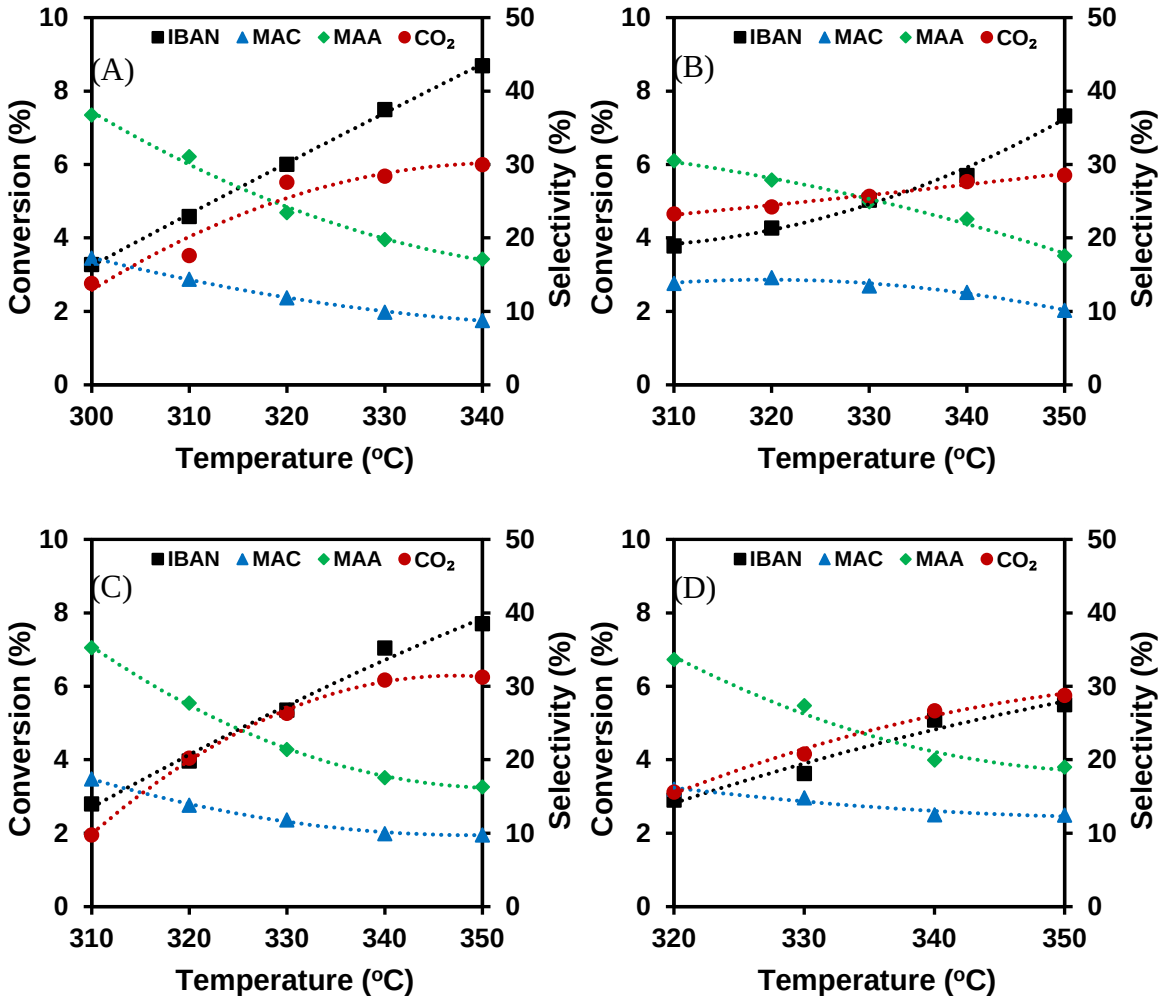

Fig. 10. Effect of the reaction temperature on the catalytic performances of (A)30CsV$_1$ catalyst, (B) 30RbV$_1$ catalyst, (C) 30CsV$_2$ catalyst, and (D) 30RbV$_2$ catalyst. (IBAN = *iso*butane, MAC = methacrolein, MAA = methacrylic acid).

Comparing the different counter-cations, the conversions of *iso*butane over the 30CsV$_1$ catalyst at different reaction temperatures were much higher than those obtained over the 30RbV$_2$ catalyst. For example, at 340°C, the conversion of *iso*butane was 8.7% for 30CsV$_1$, while for 30RbV$_2$, it was 5.1%. Hence, although there have been some reports about rubidium-doped catalysts in alcohol catalytic conversion [46,47], rubidium is not the best choice for the catalytic oxidation of *iso*butane. **Fig. 11** shows the IBAN conversion as a function of the MAC+MAA selectivity for 30CsV$_1$, 30CsV$_2$, 30RbV$_1$ and 30RbV$_2$ catalysts. The 30CsV$_1$ catalyst exhibits the highest selectivity in the main products at a given conversion, meanwhile, it possesses the highest *iso*butane conversion at a given selectivity. The trend was observed for the performance followed the order: 30CsV$_1$ > 30RbV$_1$ > 30CsV$_2$ > 30RbV$_2$.

This clearly evidenced that the use of cesium as counter cation is more favorable than rubidium and that replacing molybdenum by one vanadium is better than by two vanadium. In fact, it is known that di-vanado substituted phosphomolybdic acid is not a stoichiometric phase, since compounds with vanadium stoichiometry > 1 cannot be obtained in the pure state, but are a mixture of polyanions, which is disadvantageous for the catalytic activity [12,48,49]. Another postulate is that the decrease in activity of a catalysts at a stoichiometric vanadium content of 2 would be related to the formation of VO_2 species [48,50,51].

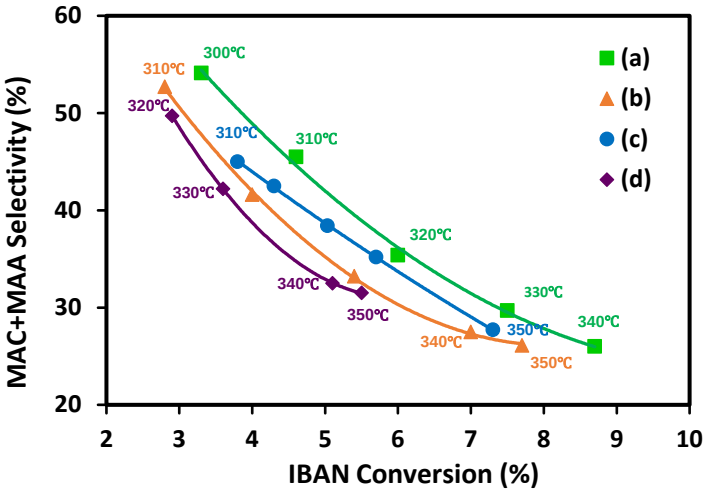

Fig. 11. Relationship between IBAN conversion and selectivity (MAC+MAA) of (a) $30CsV_1$, (b) $30CsV_2$, (c) $30RbV_1$ and (d) $30RbV_2$ catalysts at different temperatures.

The difference in the catalytic performance between CsV and RbV can be explained by taking a closer look to their respective acidities. In fact, according to the NH_3-TPD analysis, a correlation was attempted between acidity and catalytic activity, defined as follows [38]:

$$Activity = \frac{F_{IBAN} \times X_{IBAN}}{S_{BET} \times m_{cat.}}$$

where F_{IBAN} is the molar flowrate of fed *iso*butane, X_{IBAN} the *iso*butane conversion (320 °C), S_{BET} the specific surface area and $m_{cat.}$ the mass of catalyst. By plotting activity *vs.* acidity, a linear relationship was obtained (**Fig. 12**). Therefore, the number of acid sites in the $30CsV_1$ catalyst is higher than that in the other three catalysts, confirming that the acidic sites are mainly required for the C-H bond activation step [43].

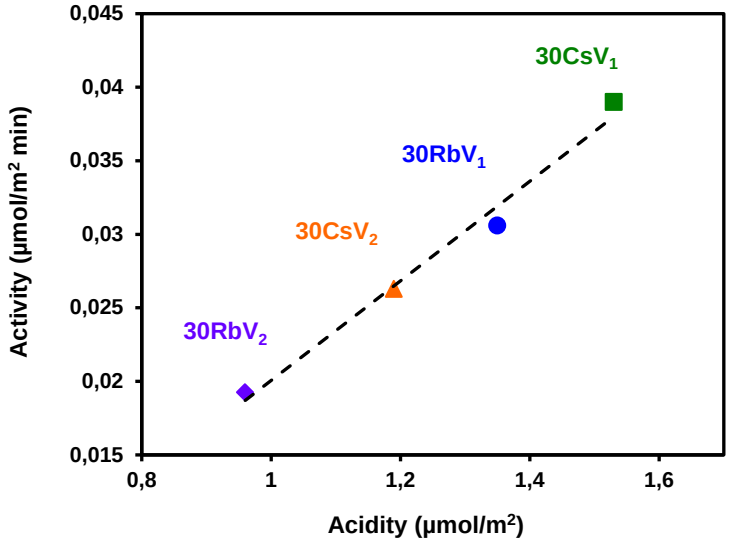

Fig. 12. Correlation between the activity in *iso*butane oxidation and the acidity of catalysts.

3.2.3 Effects of active phase amount

Following the test of different kinds of active phases, catalysts with different amounts of CsV_1, CsV_2 and RbV_2 were prepared on SiO_2 and tested at 320 °C, 330 °C and 340 °C.

The catalytic performances of the three series of catalysts with different loadings are summarized in **Tables S8 to S10**. For $10CsV_1$, the conversion of *iso*butane was quite low. The most plausible explanation is the low loading of active phase resulting in low amounts of active sites - in agreement with the low acidity found by ammonia TPD. On the other hand, it is also possible that the catalyst with low loading has poor stability, and that the catalyst is thus decomposed under the reaction conditions [31]. For the other catalysts containing 20 wt.%-50 wt.% of CsV_1 on SiO_2, the *iso*butane conversion increased (from 5.0% for $20CsV_1$ to 10.1% for $50CsV_1$), obviously with the increase in loading of active phase, indicating that the conversion of *iso*butane is proportional to the amount of active phase and the quantity of acid sites. The catalytic performances of the other two series of catalysts, CsV_2/SiO_2 and RbV_2/SiO_2, showed a similar trend. The best IBAN conversion was 8.9% for $50CsV_2$ and 7.7% for $50RbV_2$. However, the selectivity to by-products also increased with the increased amount of active phase, especially concerning the selectivity to CO_2 and acetic acid (AA). **Fig. 13** shows the selectivity to the main products of interest (MAA+MAC) for the three series of catalysts as a function of *iso*butane conversion. It clearly shows that the catalytic performances of

catalysts at a given selectivity or conversion are in the order of: CsV_1/SiO_2 ($Cs_2H_2PMo_{11}VO_{40}/SiO_2$) > CsV_2/SiO_2 ($Cs_{2.5}H_{2.5}PMo_{10}V_2O_{40}/SiO_2$) > RbV_2/SiO_2 ($Rb_{2.5}H_{2.5}PMo_{10}V_2O_{40}/SiO_2$).

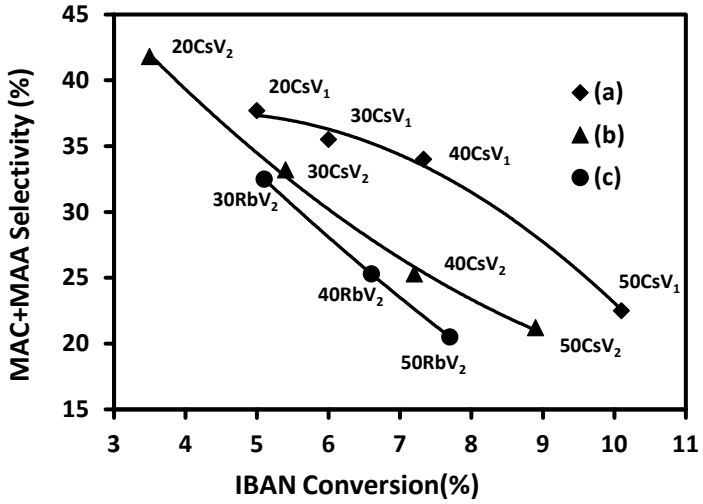

Fig. 13. Relationship between conversion and selectivity of (a) CsV_1/SiO_2 catalysts (320 °C), (b) CsV_2/SiO_2 catalysts (330 °C), (c) RbV_2/SiO_2 catalysts (340 °C) with various loadings.

It is well known that the first step in selective *iso*butane oxidation, the dehydrogenation of the tertiary carbon atoms, is the rate determining step of the reaction[14]. The acidic sites on the surface effectively promote the hydrocarbon activation and lead to the C=C bond formation by oxidative dehydrogenation. Therefore, the density of acidic sites on the catalyst surface plays a key role in the activation of *iso*butane. **Fig. 14** actually shows the relationship between the IBAN conversion and the surface acid density of these three series catalysts (CsV_1/SiO_2 catalysts, CsV_2/SiO_2 catalysts, RbV_2/SiO_2 catalysts). As one can see, the *iso*butane conversion increases when increasing the surface acidity. For lower loadings, a significant increasing was observed for cesium catalysts (10 wt.% to 20 wt.%) and rubidium catalysts (20 wt.% to 30 wt.%). However, for higher loadings, > 30 wt.%, the conversion of *iso*butane only moderately increased with the surface acid density which is in agreement with previous reports [14].

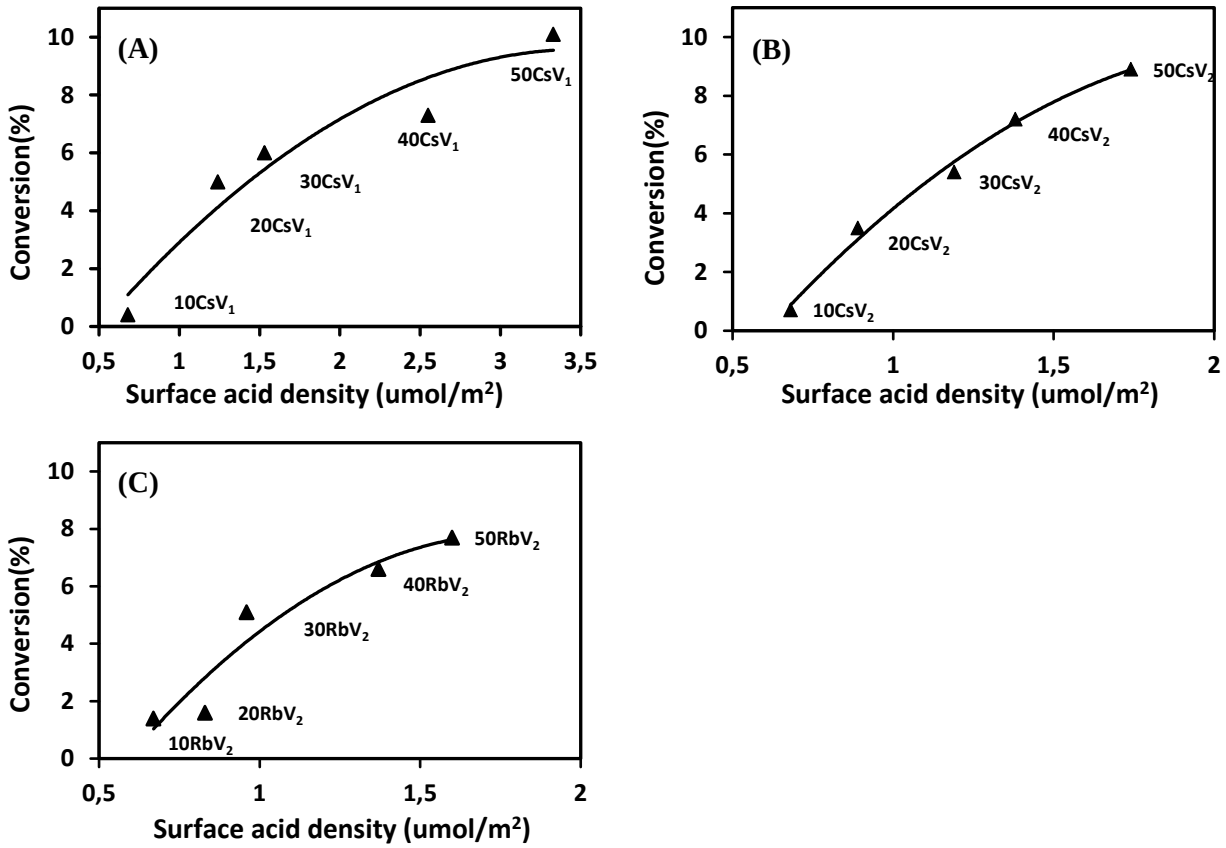

Fig. 14. Relationship between the IBAN conversion and the surface acid density over (A) CsV_1/SiO_2 catalysts (320 °C), (B) CsV_2/SiO_2 catalysts (330 °C), (C) RbV_2/SiO_2 catalysts (340 °C).

In order to determine the optimal loading of active phase, the selectivity to the main products is depicted at the same level of IBAN conversion in **Fig. 15** and summarized in **Tables S11 and S12**. According to the discussion about the effect of reaction temperature and catalytic performances on the catalytic activity in the last section, the selectivity for these series of catalysts have been compared with catalysts loaded with 30 wt.% of active phase. At the first glance one can see that, except for 10-20 wt.% catalysts, the best selectivity to the desired products (MAC+MAA) was observed for the CsV_1/SiO_2 and RbV_2/SiO_2 series with 39.1% (IBAN conversion at 6.0%) of 40 CsV_1, and 32.9% (IBAN conversion at 5.0%) of 40 RbV_2. Thus, the optimal loading is 40 wt.%. This conclusion is consistent with the characterization results showing that the 40 wt.% samples had high acidity, highest reducibility and a good dispersion of the active phase on the surface of the silica support.

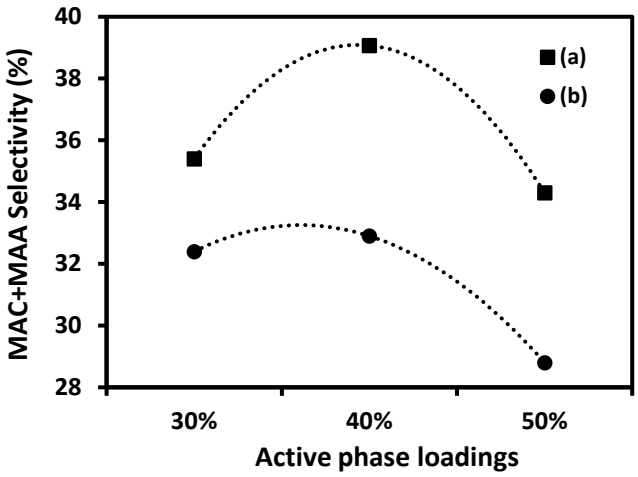

Fig. 15. Relationship between active phase loadings and selectivity of (a) CsV_1/SiO_2 catalysts (310-320 °C), (b) RbV_2/SiO_2 catalysts (330-340 °C) at the same level of IBAN conversion.

3.2.4 Long-term catalytic performance of catalyst

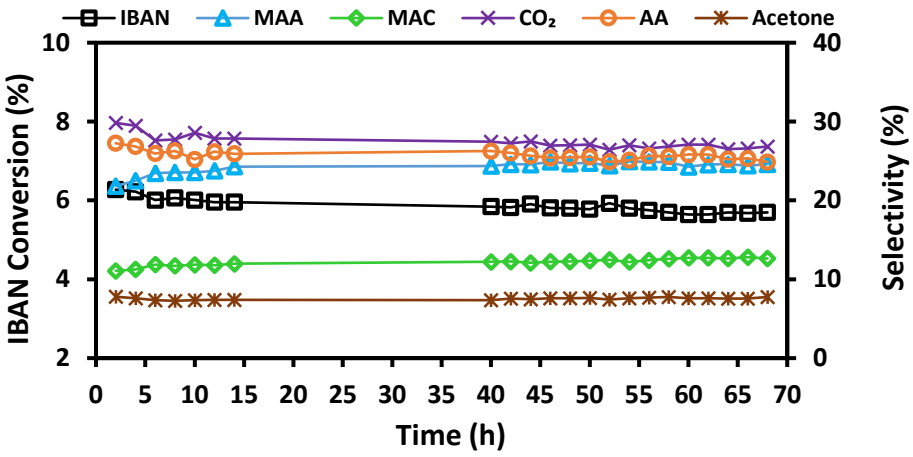

Fig. 16. Catalytic stability test over the sample $30CsV_1$ at 320 °C.

Finally, the long-term catalytic performance was evaluated for the $30CsV_1$ at 320 °C. From the results, **Fig. 16**, it can be noticed that catalyst exhibits a quite stable performance during 70 h under stream. The conversion of *iso*butane was stable at around 6 % after 4 h from the start of the reaction. Only a slight decrease in the conversion of *iso*butane from 6.2 % at the very beginning to 5.7% after 70 h was found, which is probably due to the sintering of the catalyst to form larger crystallites as evidenced by XRD and BET (108 Å for fresh and 164 Å for spent analyzed; specific surface area of 220 m^2/g for fresh and 207 m^2/g for spent).

4 Conclusions

As a conclusion, three series of Keggin-type catalysts (xCsV$_1$/SiO$_2$, xCsV$_2$/SiO$_2$ and xRbV$_2$/SiO$_2$ catalysts) with 10–50 wt.% loadings of active phase on SiO$_2$ were prepared by the impregnation method. They were characterized with different techniques (XRD, BET, TGA, Raman spectroscopy, H$_2$-TPR, and NH$_3$-TPD), and their catalytic activity in the selective oxidation of *iso*butane to methacrylic acid and methacrolein were evaluated. First, catalysts loaded with 30 wt.% of heteropoly salt were selected to assess the effect of temperature on the catalytic performances. We found that the counter cation and the degree of vanadium substitution had significant impact on the catalytic performance: Rubidium-containing catalysts require higher reaction temperatures to convert *iso*butane, which did not favor the selectivity to the desired product. Cs^+ as a counter-ion in the presence of one V achieved the higher MAA and MAC selectivities at a given level of *iso*butane conversion. In the following, the performance of the CsV$_1$/SiO$_2$, CsV$_2$/SiO$_2$ and RbV$_2$/SiO$_2$ catalysts with active phase contents ranging from 10 to 50 wt.% were studied. It followed the order: CsV$_1$/SiO$_2$ > CsV$_2$/SiO$_2$ > RbV$_2$/SiO$_2$. Moreover, it was shown that using higher contents of active phase - up to a certain extent - led to an increase in conversion. This could be explained by the fact that acidity is the key to activate the C-H bond: with the increase in the active phase loading, the surface acid sites density increased, which led to an increase in catalytic activity. Hence, the best performance was observed over the 40 wt.% samples, which not only had high acidity, but also a highly homogeneous dispersion of the active phase on the support. Within all the catalysts tested, through the above test comparison, 40CsV$_1$ has shown the best catalytic performance.

Acknowledgements

This work has benefited from the support of the CSC-Ecole Centrale de Lille PhD scholarship program. Chevreul Institute (FR 2638), Ministère de l'Enseignement Supérieur, de la Recherche et de l'Innovation, Hauts-de-France Region and FEDER are also acknowledged.

References

[1] W. Ueda, D. Vitry, T. Katou, Catal. Today 96 (2004) 235–240.

[2] G. Landi, L. Lisi, J.C. Volta, Chem. Commun. 3 (2003) 492–493.

[3] M. Misono, Top. Catal. 21 (2002) 89–96.

[4] M. Ai, J. Mol. Catal. A Chem. 114 (1996) 3–13.

[5] T. Kobayashi, Catal. Today 71 (2001) 69–76.

[6] M. Sun, J. Zhang, P. Putaj, V. Caps, F. Lefebvre, J. Pelletier, J.M. Basset, Chem. Rev. 114 (2014) 981–1019.

[7] W. Chu, J. Luo, S. Paul, Y. Liu, A. Khodakov, E. Bordes, Catal. Today 298 (2017) 145–157.

[8] V.S. Arutyunov, R.N. Magomedov, A.Y. Proshina, L.N. Strekova, Chem. Eng. J. 238 (2014) 9–16.

[9] V.F. Coindre, S.M. Kinney, M. V. Sefton, Biomaterials 259 (2020) 120324.

[10] K. Nagai, Appl. Catal. A Gen. 221 (2001) 367–377.

[11] A.W. Smith, I.T. Jackson, J. Yousefi, Eur. J. Plast. Surg. 22 (1999) 17–21.

[12] M.J. Darabi Mahboub, J.L. Dubois, F. Cavani, M. Rostamizadeh, G.S. Patience, Chem. Soc. Rev. 47 (2018) 7703–7738.

[13] S. Liu, L. Chen, G. Wang, J. Liu, Y. Gao, C. Li, H. Shan, J. Energy Chem. 25 (2016) 85–92.

[14] F. Jing, B. Katryniok, F. Dumeignil, E. Bordes-Richard, S. Paul, J. Catal. 309 (2014) 121–135.

[15] Y. Liu, J. He, W. Chu, W. Yang, Catal. Sci. Technol. 8 (2018) 5774–5781.

[16] M. Sultan, S. Paul, M. Fournier, D. Vanhove, Appl. Catal. A Gen. 259 (2004) 141–152.

[17] F. Cavani, R. Mezzogori, A. Pigamo, F. Trifirò, E. Etienne, Catal. Today 71 (2001) 97–110.

[18] J.C. Védrine, I. Fechete, Comptes Rendus Chim. 19 (2016) 1203–1225.

[19] S. Kendel, T. Brown, Catal. Letters 141 (2011) 1767–1785.

[20] E. Bordes-Richard, Catal. Today (2019) 1–12.

[21] M. Misono, Chem. Commun. 1 (2001) 1141–1153.

[22] N. Mizuno, M. Misono, Chem. Rev. 98 (1998) 199–217.

[23] D. Vanhove, Appl. Catal. A Gen. 138 (1996) 215–234.

[24] H.L. Kee, H. Tang, Angew. Chemie - Int. Ed. 30 (2013) 1–59.

[25] I. V. Kozhevnikov, Chem. Rev. 98 (1998) 171–198.

[26] S. Ganapathy, M. Fournier, J.F. Paul, L. Delevoye, M. Guelton, J.P. Amoureux, J. Am. Chem. Soc. 124 (2002) 7821–7828.

[27] L. Barcza, M.T. Pope, J. Phys. Chem. 79 (1975) 92–93.

[28] M. Misono, Catalog. Rev. 29 (1987) 269-321.

[29] T. Okuhara, N. Mizuno, M. Misono, Adv. Catal. 41 (1996) 113–252.

[30] F.X. Liu-Cai, C. Pham, F. Bey, G. Hervé, React. Kinet. Catal. Lett. 75 (2002) 305–314.

[31] M. Kanno, T. Yasukawa, W. Ninomiya, K. Ooyachi, Y. Kamiya, J. Catal. 273 (2010) 1–8.

[32] R. Al-Faze, A. Finch, E.F. Kozhevnikova, I. V. Kozhevnikov, Appl. Catal. A Gen. 597 (2020) 117549.

[33] P. Vázquez, L. Pizzio, C. Cáceres, M. Blanco, H. Thomas, E. Alesso, L. Finkielsztein, B. Lantaño, G. Moltrasio, J. Aguirre, J. Mol. Catal. A Chem. 161 (2000) 223–232

[34] G.A. Tsigdinos, C.J. Hallada, Inorg. Chem. 7 (1968) 437–441.

[35] E. Tsukuda, S. Sato, R. Takahashi, T. Sodesawa, Catal. Commun. 8 (2007) 1349–1353.

[36] I. V. Kozhevnikov, J. Mol. Catal. A Chem. 305 (2009) 104–111.

[37] S. Berndt, D. Herein, F. Zemlin, E. Beckmann, G. Weinberg, J. Schütze, G. Mestl, R. Schlögl, Berichte Der Bunsengesellschaft/Physical Chem. Chem. Phys. 102 (1998) 763–774.

[38] F. Jing, B. Katryniok, E. Bordes-richard, S. Paul, Catal. Today 203 (2013) 32-39.

[39] A. Brückner, G. Scholz, D. Heidemann, M. Schneider, D. Herein, U. Bentrup, M. Kant, J. Catal. 245 (2007) 369–380.

[40] J. He, Y. Liu, W. Chu, W. Yang, Appl. Catal. A Gen. 556 (2018) 104–112.

[41] R.C.R. Santos, D.M.V. Braga, A.N. Pinheiro, E.R. Leite, V.N. Freire, E. Longhinotti, A. Valentini, Catal. Sci. Technol. 6 (2016) 4986–5002.

[42] G Centi, F Cavani, F Trifirò, *Selective Oxidation by Heterogeneous Catalysis[M]*, Springer Science & Business Media: Berlin, Germany (2012).

[43] G. Busca, F. Cavani, E. Etienne, E. Finocchio, A. Galli, G. Selleri, F. Trifirò, J. Mol. Catal. A Chem. 114 (1996) 343–359.

[44] M. Sultan, S. Paul, D. Vanhove, Stud. Surf. Sci. Catal. 122 (1999) 283–290.

[45] S. Paul, V. Le Courtois, D. Vanhove, Ind. Eng. Chem. Res. 36 (1997) 3391–3399.

[46] M.H. Haider, N.F. Dummer, D. Zhang, P. Miedziak, T.E. Davies, S.H. Taylor, D.J. Willock, D.W. Knight, D. Chadwick, G.J. Hutchings, J. Catal. 286 (2012) 206–213.

[47] H. Shou, L. Li, D. Ferrari, D.S. Sholl, R.J. Davis, J. Catal. 299 (2013) 150–161.

[48] N. Mizuno, H. Yahiro, J. Phys. Chem. B 102 (1998) 437–443.

[49] S. Wu, Q. Kan, W. Ding, F. Shang, H. Liu, J. Guan, React. Kinet. Mech. Catal. 106 (2012) 157–164.

[50] A. Aboukaïs, D. Ghoussoub, E. Blouet-Crusson, M. Rigole, M. Guelton, Appl. Catal. A, Gen. 111 (1994) 109–118.

[51] R. Bayer, C. Marchal-Roch, F.X. Liu, A. Tézé, G. Hervé, J. Mol. Catal. A Chem. 114 (1996) 277–286.